Environmental Science & Technology

pubs.acs.org/est

Article

Reactive Iron-Bound Organic Carbon Shows Unexpected Persistence under Anoxic Burial

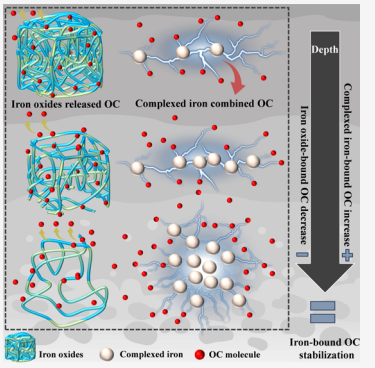
Zicheng Chen, Chenglong Wang,* Zhuoyue Zhang, Qiujun An, Tianyu Chen, Chendong Ge, Manqing Zhang, Yaping Wang, and Xinqing Zou*

Cite This: *Environ. Sci. Technol.* 2026, 60, 26504−26514

Read Online

ACCESS | Metrics & More | Article Recommendations | Supporting Information

ABSTRACT: The interaction between organic carbon (OC) and reactive iron (Fe_R) plays a critical role in suppressing OC mineralization, with the resulting Fe_R-bound OC (Fe_R-OC) constituting an important carbon sink in marine sediments. Traditional views suggest that under anoxic conditions, associations between Fe_R and OC not only enhance the OC accumulation and persistence but also inhibit the reductive dissolution of Fe_R. However, this framework leaves unresolved uncertainties regarding how Fe_R and OC mutually promote their costabilization under anoxic conditions. In this study, sequential chemical extraction was employed to distinguish organically complexed iron-bound OC (Fe_p-OC) from iron-oxide-bound OC (Fe_{ox}-OC). Our results reveal that Fe_p represents a previously underrecognized iron-associated OC pool that contributes to the OC preservation in marine sediments. Under anoxic conditions, Fe_p promotes OC retention and offsets the decline in Fe_{ox}-OC. Despite its lower abundance, Fe_p accounts for the stabilization of an average of 20.59% of the sedimentary OC. Fourier transform infrared spectroscopy (FTIR) analyses further indicate that Fe_{ox}-OC is relatively enriched in aromatic and alcohol/phenol functional groups compared with bulk OC, whereas Fe_p-OC exhibits no distinct enrichment of specific functional groups. Collectively, this study provides field-based evidence for the redistribution of OC among different Fe_R-bound fractions and highlights the potentially important contribution of Fe_p to OC preservation under anoxic conditions.



KEYWORDS: *reactive iron-bound organic carbon, carbon sink, iron reduction, complexed iron*

1. INTRODUCTION

The burial of organic carbon (OC) in marine sediments plays a pivotal role in the global carbon cycle, effectively sequestering atmospheric CO_2 into the lithosphere over geological time scales.[1−3] Moreover, in both marine and terrestrial systems, OC cycling is tightly coupled with the cycles of dissolved and mineral (oxyhydr) oxides of iron and manganese.[4,5] Reactive iron (Fe_R, defined as iron (oxyhydr) oxides reductively dissolved by sodium dithionite) can enhance the preservation of OC across diverse terrestrial and marine environments.[6,7]

OC exhibits a strong affinity for Fe_R, and the resulting reactive iron-bound OC (Fe_R-OC) complexes are considered to promote the long-term stabilization of sedimentary organic matter, a mechanism conceptualized as the "rusty sink" within the marine carbon cycle.[8−10] On a global scale, Fe_R-OC is estimated to account for approximately 21% of total organic carbon (TOC) in marine sediments, representing a major reservoir for long-term carbon sequestration.[8] However, both the size and persistence of the Fe_R-OC pool are strongly regulated by redox conditions, particularly the position of the redox boundary and the remobilization of Fe_R-OC during early diagenesis in subsurface anoxic sediment layers.[11,12]

This regulatory effect arises primarily from the pronounced redox sensitivity of iron oxides (Fe_{ox}), which constitute a major fraction of Fe_R-OC.[9,13] Laboratory studies have established that under oxic conditions, iron enhances OC preservation through the formation of short-range ordered Fe_{ox}.[14,15] In contrast, sediment incubation experiments indicate that under fluctuating redox conditions, iron can also stimulate decomposition via mechanisms such as dissimilatory iron reduction and Fenton-type reactions, thereby partly counteracting the protective role of Fe_{ox}.[16−18]

Recent studies have intriguingly shown that the proportion of sedimentary Fe_R-OC remains nearly constant over millennial time scales in anoxic marine sediments, despite substantial reductive loss of Fe_{ox} during prolonged diagenesis.[19,20] Although extensive research has established the pivotal role of Fe_{ox} in OC preservation, a fundamental question remains: how can Fe_R-OC maintain relative stability when Fe_{ox} is progressively reduced under anoxic conditions? Traditionally, Fe_R has been understood to interact with OC primarily

Received: May 23, 2026
Revised: September 2, 2026
Accepted: September 2, 2026
Published: September 8, 2026



ACS Publications © 2026 American Chemical Society

Downloaded from pubs.acs.org/esthag/article-pdf/60/37/26504/6844071 4/acs.est.6c07771.pdf by NANJING UNIV user on 25 September 2026

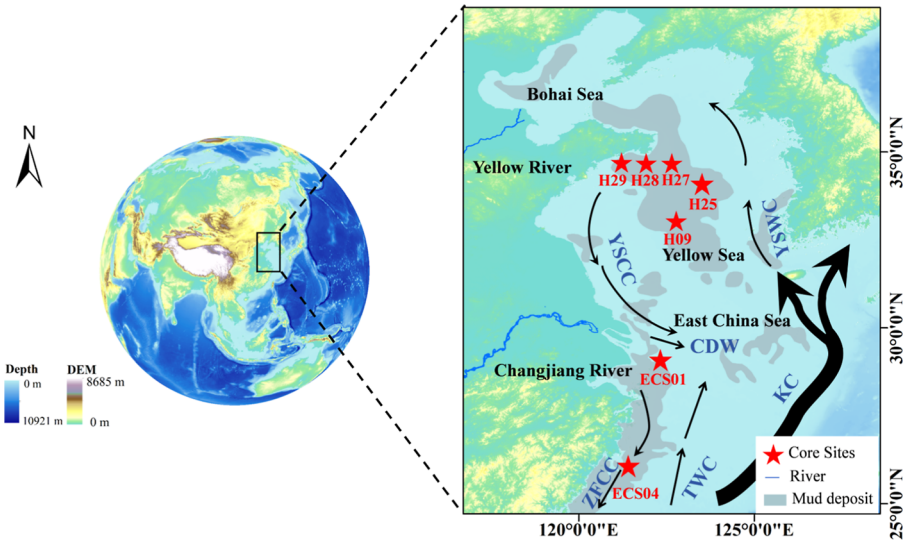


Figure 1. Schematic map of the study areas in the ECS and SYS. Black arrows indicate the redrawn circulation systems in the ECS and SYS, including the Changjiang Diluted Water (CDW), Zhejiang-Fujian Coastal Current, Taiwan Warm Current, Kuroshio Current, Yellow Sea Warm Current (YSWC), and Yellow Sea Coastal Current (YSCC). Gray shaded areas represent muddy regions, while red stars denote the sampling locations of sediment cores.

through Fe_{ox}-mediated adsorption or coprecipitation,[8,21] whereby Fe_{ox} forms protective mineral coatings that shield OC from microbial and enzymatic degradation, thereby facilitating long-term burial.[22,23] However, beyond Fe_{ox}, additional iron phases may exist within the Fe_R pool.[24,25] We hypothesize that these iron phases provide critical support and play a significant, previously underappreciated role in stabilizing Fe_R-OC complexes under anoxic conditions.

To test this hypothesis, we employed sequential extraction protocols using sodium pyrophosphate and citrate-bicarbonate-dithionite (CBD) based on the classic fractionation methods of Fe_R[8,26,27] and analyzed seven sediment cores collected from the East China Sea (ECS) and the Southern Yellow Sea (SYS; Figure 1). Using this sequential extraction approach, sedimentary Fe_R was operationally partitioned into a complexed iron phase (Fe_p) and an iron oxide phase (Fe_{ox}). The characteristics of the associated OC, together with pore water data from selected sediment cores, were subsequently analyzed. This study aims to clarify the role of Fe_p and Fe_{ox} in OC preservation and trace the fate of Fe_R-OC during anoxic burial. This study elucidates the distinct roles of different Fe_R fractions in OC sequestration and provides field-based evidence for evaluating the preservation efficiency of Fe_R-OC under anoxic conditions.

2. MATERIALS AND METHODS

2.1. Study Area and Sample Preparation

This study focuses on the inner shelf of the ECS and the central muddy deposit of the SYS (Figure 1). Annually, the Changjiang River Estuary receives substantial amounts of terrestrial particles from the Changjiang River,[28,29] making it a critically important river-dominated marginal zone and a sink for terrestrial OC in marine environments.[30] Most of the terrigenous particles carried by the CDW are transported to the ECS inner shelf by seasonal coastal currents. The Yellow Sea is situated between the Chinese mainland and the Korean peninsula. Driven by the dominant effects of the Yellow Sea Warm Current and Yellow Sea Coastal Current (Figure 1), a series of shelf mud areas have developed in this region.[31] Among these, the central mud area of the SYS exhibits distinct characteristics such as a rapid sedimentation rate and a stable depositional environment.[32]

Among these, the central mud area of SYS is characterized by a high sedimentation rate and a stable depositional environment. For this study, sediment cores were collected from contrasting settings: core ECS01 from an estuarine environment, core ECS04 from a mobile muddy area,[33] and cores H25, H27, H28, H29, and H09 from a stable muddy area.[34] Further details regarding sample collection and core characteristics are provided in Supporting Information Text S1.

2.2. Extraction of Fe-Bound OC

Detailed extraction protocols for TOC and detailed porewater sampling procedures are provided in the Supporting Information (Text S1). The CBD extraction method is primarily designed for the reductive dissolution of Fe_{ox} from sediments.[8] However, previous studies have demonstrated that CBD can also mobilize noncrystalline iron phases, which are dominated by complexed iron.[24,35] Laboratory studies suggest that this type of complexed iron phase represents a non-iron oxide precipitate formed through ligand exchange with OC and is widely distributed under reducing conditions (Supporting Information Text S2).[36,37] To ensure complete extraction, we first adopted sodium pyrophosphate to extract complexed iron (Fe_p). The sodium pyrophosphate method is widely applied for the extraction of Fe_p and has been proven to possess high extraction efficiency.[26,27,38] Afterward, the CBD method was used to extract the residual Fe_{ox}. Specific experimental details are provided in the Supporting Information (Text S3 and Figure S1).

First, Fe_p and Fe_p-bound OC (Fe_p-OC) were extracted from the sediment samples. Briefly, 0.5 g of freeze-dried sediment was treated with a 0.1 M sodium pyrophosphate solution at pH 10 to release Fe_p and Fe_p-OC into the supernatant.[26,27] The OC content in the residual sediment was defined as TOC_1, and the iron-phase content in the supernatant was measured as Fe_p.

Fe_p and Fe_p-OC were extracted using the same procedure as in the first step, followed by CBD treatment to solubilize Fe_{ox} and Fe_{ox}-OC. The OC content remaining after this second extraction was labeled TOC_2, and the supernatant iron-phase content was recorded as Fe_{ox}. To quantify the OC remobilized during extraction that was not specifically bound to Fe_R, a parallel control experiment was performed. In this control, an aliquot of the same sediment was treated identically, except that sodium dithionite and trisodium citrate in the extractant were replaced with sodium chloride of an equivalent ionic strength. The OC content in the control group was designated as TOC_0.

Calculation methods for various Fe-bound OC indicators

https://doi.org/10.1021/acs.est.6c07771
Environ. Sci. Technol. 2026, 60, 26504−26514

Downloaded from pubs.acs.org/esthag/article-pdf/60/37/26504/6844071/4/acs.est.6c07771.pdf by NANJING UNIV user on 25 September 2026

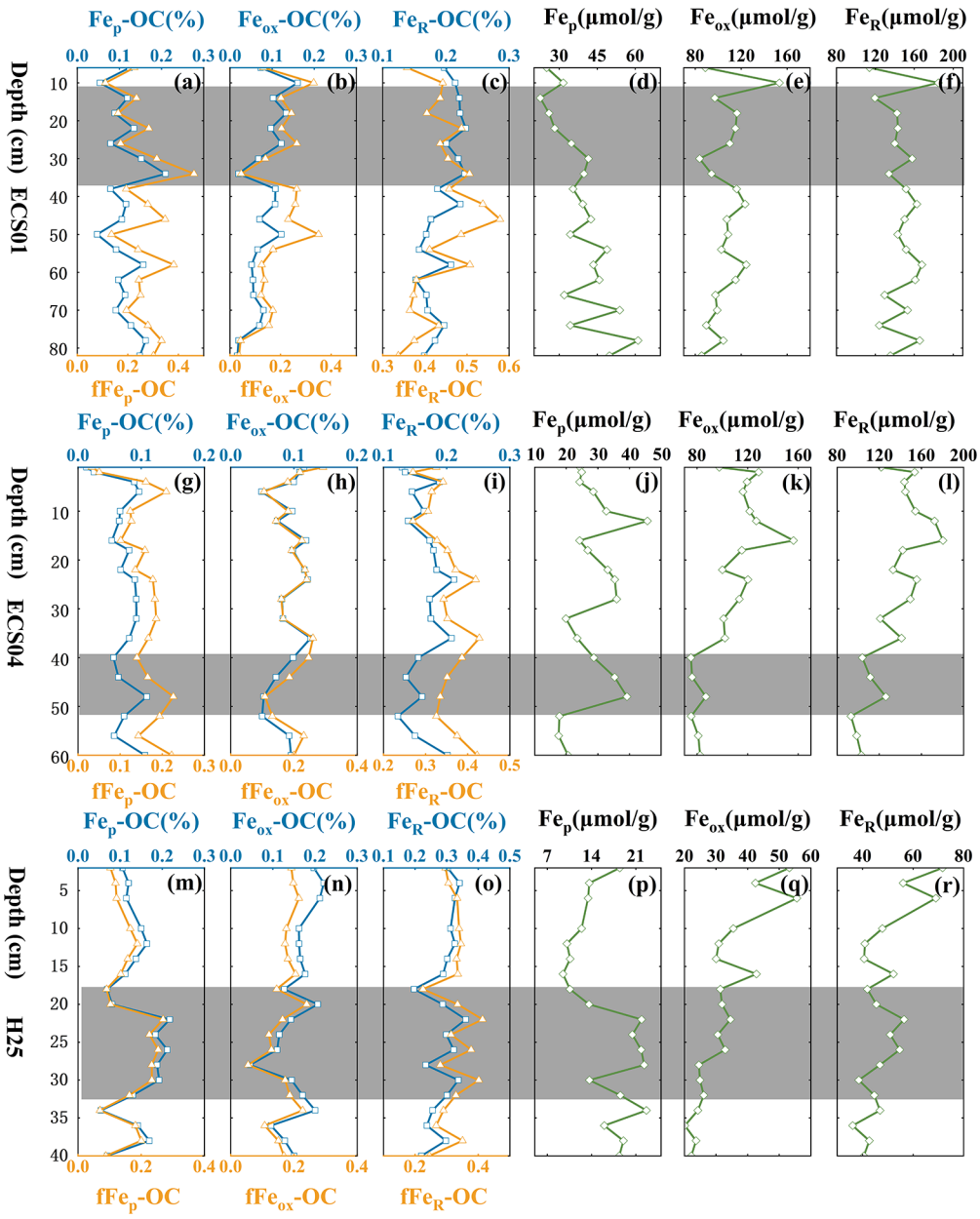


Figure 2. Distributions of Fe-bound OC fractions and iron phases in sediment cores ECS01, ECS04, and H25. Panels (a−c) show the contents of Fe_p-OC, Fe_{ox}-OC, and Fe_R-OC, respectively, together with their proportions relative to TOC in core ECS01. Blue lines indicate absolute contents, whereas yellow lines represent proportions relative to TOC; the *x*-axes are color-coded accordingly. Panels (d−f) show the contents of Fe_p, Fe_{ox}, and Fe_R, respectively. Panels (g−l) present the corresponding parameters for core ECS04, whereas panels (m−r) present those for core H25. Gray shaded areas indicate key depth intervals characterized by pronounced variations in Fe_p-OC and Fe_{ox}-OC contents, specifically 10−32 cm in core ECS01, 36−48 cm in core ECS04, and 16−30 cm in core H25.

$$Fe_R = Fe_p + Fe_{ox} \quad (1)$$

$$Fe_p - OC = TOC_0 - TOC_1 \quad (2)$$

$$Fe_{ox} - OC = TOC_1 - TOC_2 \quad (3)$$

$$Fe_R - OC = (Fe_p - OC) + (Fe_{ox} - OC) \quad (4)$$

$$fFe_R - OC(\%) = \frac{Fe_R - OC}{TOC} \times 100\% \quad (5)$$

$$fFe_p - OC(\%) = \frac{Fe_p - OC}{TOC} \times 100\% \quad (6)$$

$$fFe_{ox} - OC(\%) = \frac{Fe_{ox} - OC}{TOC} \times 100\% \quad (7)$$

where Fe_R represents the total content of reactive iron; Fe_p-OC denotes the content of Fe_p-bound OC in sediments; Fe_{ox}-OC represents the content of Fe_{ox}-bound OC in sediments; Fe_R-OC indicates the content of Fe_R-OC in sediments; fFe_p-OC stands for the mass fraction of Fe_p-OC relative to TOC; fFe_{ox}-OC refers to the mass fraction of Fe_{ox}-OC relative to TOC; and fFe_R-OC signifies the mass fraction of Fe_R-OC relative to TOC.

2.3. FTIR Spectroscopy Analysis

Following the three treatments (control, complexed, and CBD), the residual sediment samples were thoroughly mixed with potassium bromide (KBr) at a mass ratio of 1:100 and finely ground to ensure a

Downloaded from pubs.acs.org/esthag/article-pdf/60/37/26504/6844071 4/acs.est.6c07771.pdf by NANJING UNIV user on 25 September 2026

https://doi.org/10.1021/acs.est.6c07771
Environ. Sci. Technol. 2026, 60, 26504−26514

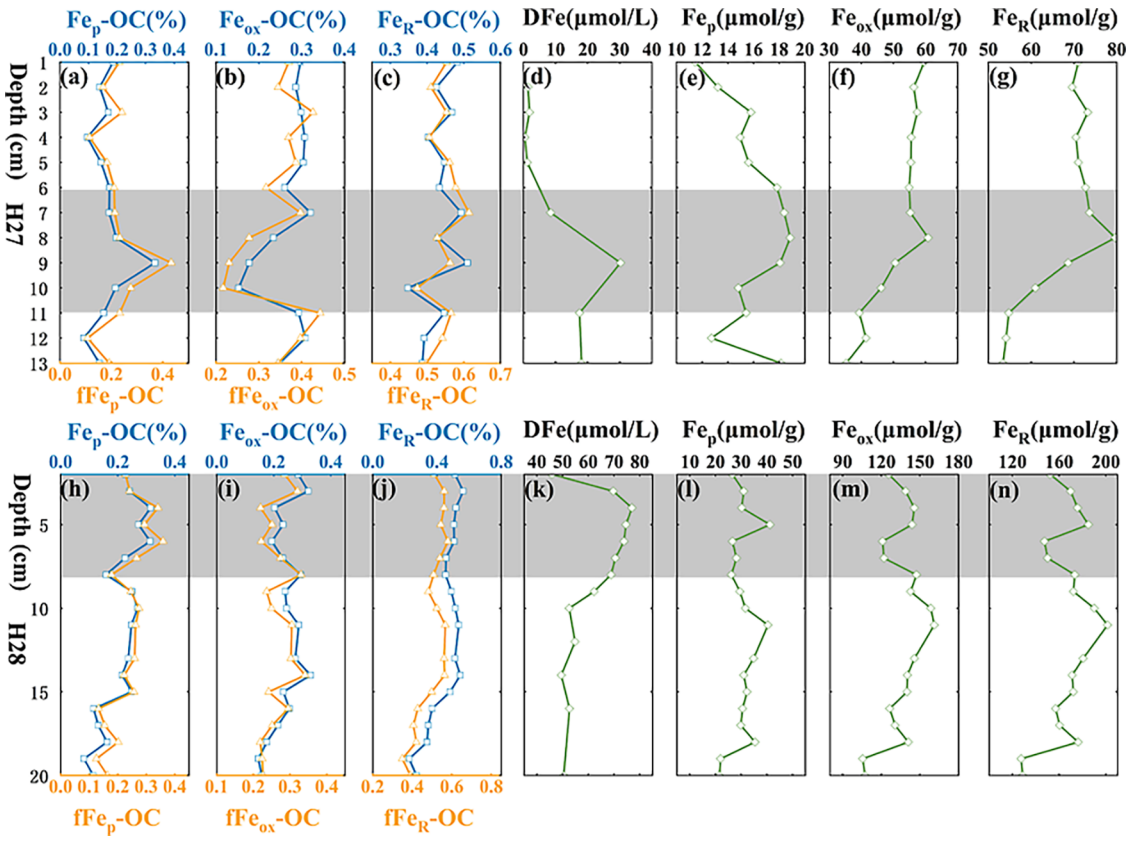


Figure 3. Distributions of Fe-bound OC fractions, porewater dissolved iron, and iron phases in sediment cores H27 and H28. Panels (a−c) show the contents of Fe_p-OC, Fe_{ox}-OC, and Fe_R-OC, respectively, together with their proportions relative to TOC in core H27. Blue lines indicate absolute contents, whereas yellow lines represent proportions relative to TOC; the *x*-axes are color-coded accordingly. Panels (d−g) show the contents of porewater dissolved iron, Fe_p, Fe_{ox}, and Fe_R, respectively. Panels (h−n) present the corresponding parameters for core H28. Gray shaded areas indicate key depth intervals characterized by pronounced variations in Fe_p-OC and Fe_{ox}-OC contents, specifically 5−10 cm in core H27 and 1−7 cm in core H28.

homogeneity. Fourier transform infrared (FTIR) spectra were collected by using a Nicolet iN10 infrared spectrometer (Thermo Scientific, USA). Spectra were acquired over the range of 4000−500 cm^{-1} at a resolution of 4 cm^{-1}, with 64 scans coadded per spectrum to improve the signal-to-noise ratio.

After subtraction of the ambient air background, the relative peak area (rA %) of each functional group was calculated as the ratio of its individual peak area to the total integrated spectral peak area.[39,40] Given the weak intensities of other spectral peaks, only the peak areas of carbohydrate-C (1050 cm^{-1}), aromatic-C (1630 cm^{-1}), and alcohol/phenol-C (3450 cm^{-1}) were summed to define the total peak area, thereby eliminating the interference of miscellaneous peaks. The ratio of aromatic-C (stable carbon component; rA_{1630}) to carbohydrate-C (labile carbon component; rA_{1050}) was then determined to assess sediment chemical stability, following established methods.[41] Higher $rA_{1630}/_{1050}$ ratios indicate greater molecular condensation and structural complexity.[42]

2.4. Statistics

Statistical analyses were performed using IBM SPSS Statistics (version 25.0; IBM Corp., Armonk, NY, USA). Pearson's correlation analysis was used to examine the linear relationship between variables and sediment depth, with statistical significance defined as $p < 0.05$, whereas $p > 0.1$ indicates that the variable shows no significant trend with depth. Due to non-normal data distribution, differences in carbon-to-iron molar ratios among Fe-bound OC fractions were assessed using the Mann−Whitney U test. All tests were two-tailed, and the significance level was set at $\alpha = 0.05$.

3. RESULT

3.1. Vertical Characteristics of Fe-Bound OC

The TOC contents of sediment cores ECS01, ECS04, and H25 ranged from 0.30% to 0.55%, 0.37% to 0.55%, and 0.83% to 1.11%, respectively, with mean values of 0.44 ± 0.06%, 0.47 ± 0.05%, and 0.91 ± 0.07% (Supporting Information Figure S2). In sediment cores H27 and H28, TOC contents ranged from 0.66% to 0.84% and 0.65% to 1.01%, respectively, with corresponding mean values of 0.77 ± 0.05% and 0.89 ± 0.09% (Supporting Information Figure S3).

Fe_R-OC contents at stations ECS01, ECS04, and H25 ranged from 0.15% to 0.23%, 0.12% to 0.21%, and 0.19% to 0.36%, respectively, with mean values of 0.19 ± 0.02%, 0.16 ± 0.01%, and 0.29 ± 0.04% (Figure 2c,i,o). At stations H27 and H28, Fe_R-OC contents ranged from 0.34% to 0.51% and 0.22% to 0.56%, respectively, with corresponding mean values of 0.43 ± 0.05% and 0.45 ± 0.09% (Figure 3c,j). No clear depth-related trend was observed at stations ECS01, ECS04, H25, H27, and H28 (Pearson, $p > 0.1$).

At stations ECS01, ECS04, and H25, fFe_R-OC ranged from 33.66% to 57.83%, 27.00% to 42.75%, and 22.48% to 41.34%, respectively, with mean values of 43.82 ± 6.32%, 34.80 ± 4.37%, and 32.12 ± 4.60% (Figure 2c,i,o). At stations H27 and H28, fFe_R-OC ranged from 47.32% to 61.41% and 34.97% to 58.02%, respectively, with mean values of 54.19 ± 3.63% and 49.99 ± 6.91% (Figure 3c,j).

https://doi.org/10.1021/acs.est.6c07771
Environ. Sci. Technol. 2026, 60, 26504−26514

Downloaded from pubs.acs.org/esthag/article-pdf/60/37/26504/6844071 4/acs.est.6c07771.pdf by NANJING UNIV user on 25 September 2026

The mean Fe_p-OC contents at stations ECS01, ECS04, and H25 were 0.11 ± 0.03%, 0.07 ± 0.02%, and 0.14 ± 0.04%, respectively (Figure 2a,g,m), whereas those at stations H27 and H28 were 0.16 ± 0.05% and 0.21 ± 0.06%, respectively (Figure 3,h). The mean Fe_{ox}-OC contents at stations ECS01, ECS04, and H25 were 0.07 ± 0.03%, 0.09 ± 0.02%, and 0.15 ± 0.04%, respectively (Figure 2b,h,n), while the corresponding values at stations H27 and H28 were 0.26 ± 0.05% and 0.24 ± 0.05%, respectively. The mean fractions of fFe_p-OC at stations ECS01, ECS04, and H25 were 25.72 ± 8.38%, 15.29 ± 5.00%, and 16.65 ± 5.96%, respectively (Figure 2a,g,m), whereas those at stations H27 and H28 were 21.81 ± 7.73% and 23.38 ± 6.36%, respectively (Figure 3a,h).

The key intervals characterized by opposing trends between the two Fe-bound OC fractions were identified (Figure 2, gray shading). In sediment cores ECS01, ECS04, and H25, Fe_{ox}-OC content exhibited a decreasing trend with depth (Pearson, $p < 0.05$), and fFe_{ox}-OC also declined significantly (Pearson, $p < 0.05$; Figure 2b,h,n). In contrast, Fe_p-OC content in these three cores showed an increasing trend (Pearson, $p < 0.05$, $p > 0.1$, and $p < 0.05$ for ECS01, ECS04, and H25, respectively), while fFe_p-OC displayed a corresponding increase (Pearson, $p < 0.05$, $p > 0.1$, and $p < 0.05$, respectively; Figure 2a,g,m). However, the increasing trends in both Fe_p-OC content and fFe_p-OC in core ECS04 were not statistically significant, as discussed in the subsequent sections.

Meanwhile, in sediment cores H27 and H28, both Fe_p-OC content and the proportion of fFe_p-OC increased sharply at depths corresponding to a dramatic rise in dissolved iron (term collectively referring to ferrous ions and ferric ions) concentrations (Figure 3a,h,d,k, gray shading), whereas marked depletion was observed in both Fe_{ox}-OC and fFe_{ox}-OC (Figure 3b,i).

3.2. Carbon−Iron Molar Ratios of Each Fe-Bound OC Fraction

The molar ratio of Fe-bound OC to Fe (OC:Fe) serves as a key indicator of the association capacity between iron and OC.[43] The mean OC:Fe ratios of Fe_R-OC at stations ECS01, ECS04, H25, H27, and H28 were 1.12 ± 0.20, 1.05 ± 0.22, 5.11 ± 0.91, 5.46 ± 0.64, and 2.26 ± 0.39, respectively (Figure 5a−e). A pronounced contrast was observed between the two Fe-bound OC fractions. The OC:Fe ratios of Fe_p-OC (2.60 ± 0.99, 2.26 ± 0.97, 7.87 ± 3.18, 8.85 ± 2.79, and 5.82 ± 1.78, respectively; Figure 5a−f) substantially exceeded those of Fe_{ox}-OC (0.61 ± 0.25, 0.74 ± 0.20, 4.00 ± 1.23, 4.45 ± 1.09, and 1.47 ± 0.26, respectively; Figure 5a−f) across the corresponding cores (Mann−Whitney U test, $p < 0.001$).

3.3. Chemical Analysis of Each Fe-Bound OC Fraction

In spectral analyses, the relative peak area of each functional group is considered to be indicative of its relative abundance. The abundance of aliphatic compounds, represented by the absorption band at 1438 cm^{-1}, exhibited no significant variation among the complexed extraction, CBD, and control treatments, likely because these compounds contributed only marginally to the overall sediment spectra (Figure 6b). Compared with the control treatment, complexed extraction did not significantly affect the relative abundances of the three identified functional groups (Figure 6c). In contrast, compared with the residue after complexed extraction, CBD treatment substantially reduced the relative abundances of aromatic-C and alcohol/phenol-C, as evidenced by the decreased intensities of the absorption bands at 1630 cm^{-1} and 3450 cm^{-1}, respectively (Figure 6c).

The OC remaining after sodium pyrophosphate extraction exhibited no significant difference in overall stability compared to bulk sediment OC (Figure 6d). In contrast, the OC retained after CBD extraction showed lower stability than the residue remaining after sodium pyrophosphate extraction alone (Figure 6d), suggesting that Fe_{ox}-OC comprises relatively more stable components. Collectively, these findings indicate that Fe_p-OC has a stability comparable to that of bulk OC, whereas Fe_{ox}-OC exhibits a greater stability than Fe_p-OC.

4. DISCUSSION

4.1. Contrasting Fates of Fe_R-OC Fractions during Burial

Sequential iron extraction enables clear differentiation of discrete iron phases and serves as a critical tool for clarifying their distinct roles in OC stabilization. Two key observations emerge from our data: (i) Fe_p-OC content and the fractional contribution of Fe_p-OC (fFe_p-OC) exhibited upward trends within key intervals of each sediment core; and (ii) concomitant depletions were observed in Fe_{ox}-OC content and its fractional contribution (fFe_{ox}-OC) over the same intervals (Figures 2 and 3).

In fact, we cannot entirely rule out the possibility that distinct signals in key intervals of all cores are related to source input changes, but this scenario is highly unlikely. The variations in Fe_R-OC in the estuarine shelf region are generally ascribed to three main reasons: (1) the effect of biogeochemical processes occurring during anoxic burial on Fe_R-OC;[14,44] (2) the varying contribution of terrestrial and marine sedimentary OC provenance;[9,10] and (3) fluctuations in the input of Fe_R or OC. These factors modify the Fe_R-OC content in sedimentary sequences.[33]

Biogeochemical processes significantly influence the preservation of carbon isotopes within these key intervals.[11] However, cores ECS01 and ECS04, located in the estuary, are heavily impacted by terrestrial inputs, and pore water data for core H25 are absent. These limitations complicate the determination of whether the two Fe-bound OC fractions are governed by biogeochemical processes. To address this issue, we supplemented $\delta^{13}C$ and C/N ratio data from cores ECS01, ECS04, and H25 to evaluate the stability of terrestrial inputs (Supporting Information Figure S2).[45] The results indicated that both $\delta^{13}C$ values and C/N ratios showed no significant variations within the key intervals across the three cores (Pearson, $p > 0.1$), suggesting that the relative contributions of terrestrial and marine sources to these sediment cores likely did not experience substantial variations.[46] In addition, within the key intervals, the Fe_p content displayed an increasing trend in cores ECS01, ECS04, and H25 (Pearson, $p < 0.05$, Figure 2d,j,p), while Fe_{ox} showed a decreasing trends (Pearson, $p < 0.05$, $p > 0.1$, $p < 0.05$, respectively, Figure 2e,k,q).

Although the variation in Fe_{ox} in core ECS04 was not statistically significant, its content decreased markedly, relative to the overlying sediment layer. We suggest that changes in iron fractions driven by terrestrial inputs should increase or decrease synchronously, rather than exhibit opposing trends.[33] In cores H27 and H28, Fe_p increased significantly during the sharp rise in porewater dissolved iron concentrations (Pearson, $p < 0.05$, Figure 3e,l), whereas a significant depletion of Fe_{ox} was also observed within the iron−manganese reduction zone, although the magnitude of this decrease was relatively small

Downloaded from pubs.acs.org/esthag/article-pdf/60/37/26504/6844071/4/acs.est.6c07771.pdf by NANJING UNIV user on 25 September 2026

https://doi.org/10.1021/acs.est.6c07771
Environ. Sci. Technol. 2026, 60, 26504−26514

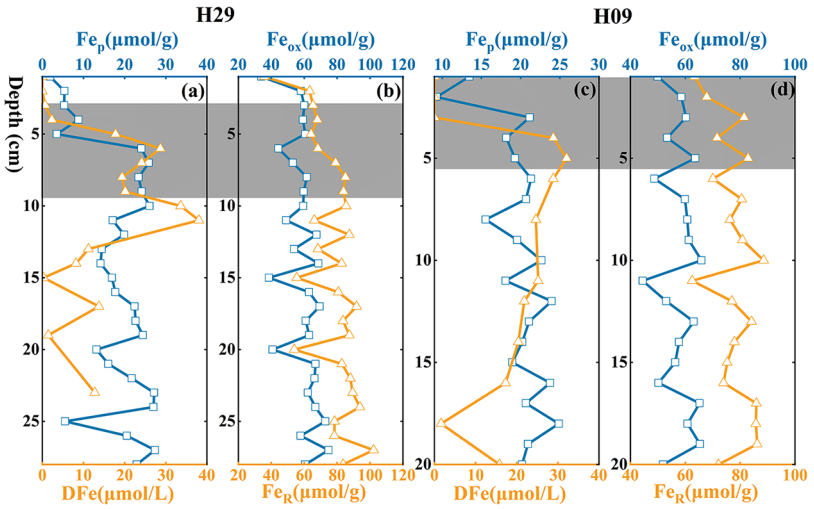


Figure 4. Distributions of porewater dissolved iron and iron fractions in sediment cores H29 and H09. (a) Profiles of Fe_p and porewater dissolved iron in core H29. The blue line represents Fe_p, and the yellow line represents dissolved iron; the *x*-axes are color-coded accordingly. (b) Profiles of Fe_{ox} and Fe_R in core H29. The blue line represents Fe_{ox}, and the yellow line represents Fe_R. (c) Profiles of Fe_p and dissolved iron in core H09. (d) Profiles of Fe_{ox} and Fe_R in core H09. The gray shaded areas indicate the sediment layers where iron reduction occurred.

(Figure 3f,m). The sharp increase in dissolved iron concentrations within sediment porewater is an important indicator for identifying intense Fe_{ox} reduction, and such sedimentary intervals defined the iron reduction zone (Figure 3, gray shading).

We speculate that, following the reduction of Fe_{ox} in sediments, resuspension of surface sediments promotes the reoxidation of dissolved iron. Therefore, pronounced depletion of Fe_{ox} is difficult to observe within the iron reduction zones of cores H27 and H28.[33] Our pore water data further confirm the occurrence of intensive Fe_{ox} reduction. In cores ECS01, ECS04, and H25, Fe_{ox} reduction occurred in relatively deep sediment layers, whereas the influence of sediment resuspension was limited to shallow depths. Consequently, dissolved iron could not be effectively reoxidized to form Fe_{ox}, resulting in a substantial depletion of Fe_{ox} in these sediments. Taken together, these lines of evidence suggest that biogeochemical processes may be the primary drivers of the distinct variation patterns observed in Fe_p-OC and Fe_{ox}-OC associations. This observation raises a key question: why do Fe-bound OC fractions exhibit contrasting variation trends following anoxic burial?

The observed depletion of Fe_{ox}-OC may largely stem from the reductive dissolution of Fe_{ox}.[14,44] Following anoxic burial, Fe_{ox} undergoes two concurrent reductive pathways: microbial dissimilatory iron reduction and sulfide-mediated chemical reduction.[47,48] Together, these processes reduce Fe(III) to Fe(II) and are accompanied by the degradation of mineral crystal structures. Dissimilatory iron-reducing bacteria utilize Fe(III) as a terminal electron acceptor, oxidizing organic matter to conserve energy.[48,49] In contrast, sulfide-mediated chemical reduction is driven primarily by hydrogen sulfide (H_2S/HS^-) produced by sulfate-reducing bacteria, which reacts abiotically with Fe_{ox} through redox reactions.[50] Another possible explanation for the decrease in fFe_{ox}-OC and Fe_{ox}-OC content with increasing depth may be related to the predominance of more crystalline Fe_{ox} in the Fe_{ox} pool beneath the surface sediments.[51] The maturation of these Fe_{ox} may result in the release of previously associated OC, thereby contributing to Fe_{ox}-OC loss.[23,52] These two mechanisms are not mutually exclusive and could act in combination. OC bound to Fe_{ox}, when released, may either remain in the dissolved OC pool or the sediment OC pool or undergo mineralization,[53,54] with labile OC molecules decomposing into inorganic carbon and smaller molecular substances.[55]

The accumulation of Fe_p-OC is likely governed by the ligand-binding mode of Fe_p. Previous studies have suggested that iron ions (used here to collectively refer to ferrous and ferric ions) produced during the reductive dissolution of Fe_{ox} can be re-immobilized onto the surfaces of metal oxide minerals through coordination bonding. In this process, they interact with surface hydroxyl groups (−OH) on mineral crystals to form stable Fe_p species.[56−58] This binding mode prevents iron ions from precipitating independently or persisting in a free dissolved state, thereby promoting their reassociation with solid-phase sediments in the form of coordination complexes.[37] Experimental evidence further indicates that Fe_p, with iron ions as coordination centers, can bind to oxygen-rich functional groups in organic ligands (e.g., carboxyl groups). Fe_p can also effectively adsorb OC through coordination interactions with hydroxyl groups in organic matter.[26,27,36] This coupled mechanism provides a plausible explanation for the vertical variations in the two Fe-bound OC fractions observed across the five sediment cores.

Therefore, on the basis of previous studies and our field observations, we propose the following potential mechanism to explain the concurrent decrease in Fe_{ox}-OC and increase in Fe_p-OC observed in this study. During the reductive dissolution of Fe_{ox}, the mineral structure is disrupted, leading to the release of Fe_{ox}-OC and dissolved iron. The released iron subsequently readsorbs onto metal oxide surfaces within the sediment, where it forms Fe_p through coordination interactions and continuously associates with OC via ligand exchange and related processes, resulting in concurrent increases in both Fe_p and Fe_p-OC. Although no significant increase in Fe_p-OC was observed within the key depth interval of core ECS04, the Fe_p content increased markedly. We attribute this discrepancy to the relatively low TOC content in ECS04 (Supporting Information Figure S2), which likely limits the absolute

https://doi.org/10.1021/acs.est.6c07771
Environ. Sci. Technol. 2026, 60, 26504−26514

Downloaded from pubs.acs.org/esthag/article-pdf/60/37/26504/6844071/4/acs.est.6c07771.pdf by NANJING UNIV user on 25 September 2026

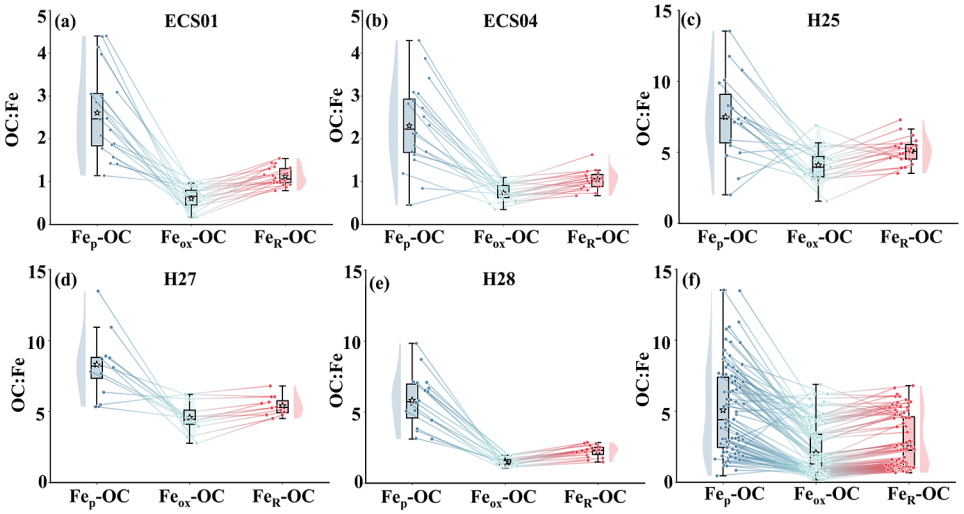


Figure 5. Molar OC:Fe ratios of Fe$_p$-OC, Fe$_{ox}$-OC, and Fe$_R$-OC. (a–e) Molar OC:Fe ratios of ECS01, ECS04, H25, H27, and H28, respectively. (f) Molar OC:Fe ratios of all cores.

abundance of Fe$_p$-OC and thereby obscures its increasing trend.

This phenomenon is consistent with observations from the iron reduction zones of sediment cores H27 and H28, where elevated dissolved iron concentrations coincided with the marked enrichment of Fe$_p$. To further evaluate the relationship between iron redox cycling and the enrichment of Fe$_p$, additional data from sediment cores H29 and H09 were included in the analysis. Sequential chemical extraction of Fe$_p$ and Fe$_{ox}$ revealed pronounced Fe$_p$ enrichment within the iron reduction zones (Figure 4a,c, gray shaded areas). In core H29, the Fe$_{ox}$ content decreased substantially across the reduction zone (Figure 4b), whereas little variation was observed in core H09 (Figure 4d). This discrepancy is most likely attributable to the reoxidation of dissolved iron followed by the reformation of Fe$_{ox}$. Collectively, these findings provide field-based evidence that OC is redistributed among different Fe$_R$-bound fractions during iron redox cycling.

To further validate the temporal trends of different irons phases and their associated OC fractions under anaerobic conditions, we conducted a laboratory incubation experiment (Supporting Information Text S4 and Figures S5 and S6). Natural sediments were amended with different concentrations of ferrihydrite–glucose complexes (Supporting Information Tables S1 and S2), and the temporal changes in individual iron phases and their associated OC fractions were monitored. The incubation results showed that, under anaerobic conditions, dissolved iron concentrations in sediment porewater increased continuously, Fe$_{ox}$-OC contents gradually decreased, whereas Fe$_p$ and Fe$_p$-OC contents increased (Supporting Information Figure S6). Overall, the temporal trends observed during laboratory incubation were broadly consistent with those identified in the field.

Taken together, these observations reveal a key finding: the apparent stability of the total Fe$_R$-OC pool does not necessarily reflect a constant composition of its constituent fractions. Instead, the overall Fe$_R$-OC pool is sustained through the redistribution of OC among different Fe$_R$-bound fractions. As anoxic conditions intensify, Fe$_{ox}$ and Fe$_{ox}$-OC are progressively depleted. Concurrently, Fe$_p$ and Fe$_p$-OC accumulate, thereby offsetting the loss of Fe$_{ox}$-OC and thereby preserving the overall Fe$_R$-OC pool.

4.2. Fe$_p$-OC Constitutes a Key Fraction of OC in Marine Sediments

Although Fe$_{ox}$ is the dominant iron phase in the sediments of the study area, the proportion of Fe$_{ox}$-OC in Fe$_R$-OC is lower than the contribution of Fe$_{ox}$ to Fe$_R$ (Supporting Information Figure S3f–j). Similarly, the contribution of Fe$_p$-OC to Fe$_R$-OC is markedly higher than that of Fe$_p$ to Fe$_R$ (Supporting Information Figure S3a–e).[23,59] On average, 20.59 ± 6.68% of OC remains associated with Fe$_p$ below the oxygenated surface sediment layer. This finding indicates that Fe$_p$ acts as a non-negligible metal carrier for carbon sequestration. The higher carbon-to-iron molar ratios of Fe$_p$-OC (Figure 5a–f) suggest that Fe$_p$ stabilizes OC through a mechanism distinct from those of clay minerals or crystalline metal oxides.

The formation of Fe$_p$-OC requires a supply of iron ions, which act as binding carriers and form coordinate bonds with oxygen-containing functional groups in organic matter.[36,37] This mechanism differs fundamentally from that of crystalline Fe$_{ox}$, which stabilizes the OC primarily through coprecipitation or adsorption. Coprecipitation occurs when OC molecules intercalate into the crystal lattice and become incorporated into Fe$_{ox}$ crystals during the reoxidation of the iron ions. In contrast, adsorption involves interactions between hydroxyl groups on the crystal surface and OC functional groups via cation bridging, ligand exchange, and other pathways.[60,61] Under anoxic conditions, reductive dissolution of Fe$_{ox}$ releases dissolved iron ions, thereby increasing the availability of coordination centers and potentially promoting the formation of Fe$_p$-OC. Consequently, the association of OC with Fe$_p$ may represent an important, yet previously underappreciated, pathway for OC preservation under anoxic conditions in marine sediments.

4.3. Variations in OC Associations across Iron Phases

OC loading in marine environments via sediment transport is characterized by recalcitrant organic compounds such as alcohols/phenols and aromatic hydrocarbons.[62,63] Conversely, marine organic matter produced in situ is rich in amino acids and carbohydrates from phytoplankton.[64] FTIR analyses further suggest that, compared with bulk sediment OC, Fe$_{ox}$-OC exhibits distinct variations in infrared absorption bands associated with different functional groups, particularly

https://doi.org/10.1021/acs.est.6c07771
Environ. Sci. Technol. 2026, 60, 26504–26514

Downloaded from pubs.acs.org/esthag/article-pdf/60/37/26504/6844071/4/acs.est.6c07771.pdf by NANJING UNIV user on 25 September 2026

aromatic and alcohol/phenol functional groups. Specifically, the relative abundances of aromatic-C and alcohol/phenol-C decreased following CBD extraction, as reflected by the reduced areas of the corresponding absorption bands. In contrast, Fe_p-OC exhibited no distinct FTIR signatures indicative of enrichment in specific functional groups (Figure 6c).

We hypothesize that the observed shifts in spectral signatures are attributable to the distinct structural properties of diverse iron mineral phases.[54,65] Prior investigations have documented that recalcitrant organic moieties enriched in aromatic frameworks and alcohol/phenol lignin degradation products exhibit a greater tendency toward adsorption and coprecipitation with Fe_{ox} relative to those of aliphatic compounds. Furthermore, aromatic organic matter is capable of forming aromatic-Fe_{ox} complexes with Fe_{ox}, which facilitates its selective preservation at sediment aggregate interfaces.[66,67]

The association between Fe_p and OC is primarily mediated through coordination interactions between the iron ions and oxygen-containing functional groups. Previous studies have shown that oxygen-rich functional groups, such as carboxyl, hydroxyl, and ketone groups, can undergo deprotonation to generate reactive binding sites, which subsequently form stable complexes with iron ions.[26,68] However, Fe_p-OC did not exhibit distinct FTIR signatures indicative of enrichment in any specific oxygen-containing functional groups. This observation suggests that the association between Fe_p and the OC is not governed by a single type of functional group. Instead, multiple binding sites, including carboxyl groups associated with aromatic structures,[37] may collectively contribute to complexation, thereby preventing the emergence of distinct FTIR signatures associated with any individual functional group.

Carbon chemical analyses further support this contrast, demonstrating that Fe_{ox}-OC is generally more chemically stable than Fe_p-OC (Figure 6d). In addition, no significant difference in chemical stability was observed between Fe_p-OC and bulk sediment OC (Figure 6d). The greater stability of Fe_{ox}-OC may also reflect the effects of prolonged fluvial transport. During transport, the more labile OC associated with Fe_{ox} is preferentially degraded, resulting in the relative enrichment of recalcitrant organic compounds such as terrestrial lignin derivatives and aromatic phenolic acids.[69]

5. IMPLICATIONS

Fe_R comprises two major fractions, Fe_{ox} and Fe_p, each playing a distinct role in OC preservation under anoxic conditions. In anoxic sediments, Fe_p-OC accounts for an average of 20.59 ± 6.68% of TOC. During anoxic burial, Fe_{ox} is progressively depleted, resulting in the release and remobilization of Fe_{ox}-OC from mineral surfaces. In contrast, the Fe_p pool increases substantially, accompanied by a corresponding increase in Fe_p-OC. When OC reassociates with Fe_p, it is rapidly removed from the microbially accessible dissolved OC pool, thus slowing OC remineralization. This process promotes the transfer of OC to deeper layers, ultimately reducing OC mineralization or decomposition during geochemical processes such as early diagenesis.

In addition, significant reductions were observed in the peak areas of aromatic and alcohol/phenol functional groups following the Fe_{ox} extraction. These results suggest that Fe_{ox}-OC is enriched in aromatic-C and alcohol/phenol-C, whereas Fe_p-OC exhibits no distinct enrichment in specific OC functional groups. Overall, these findings not only provide

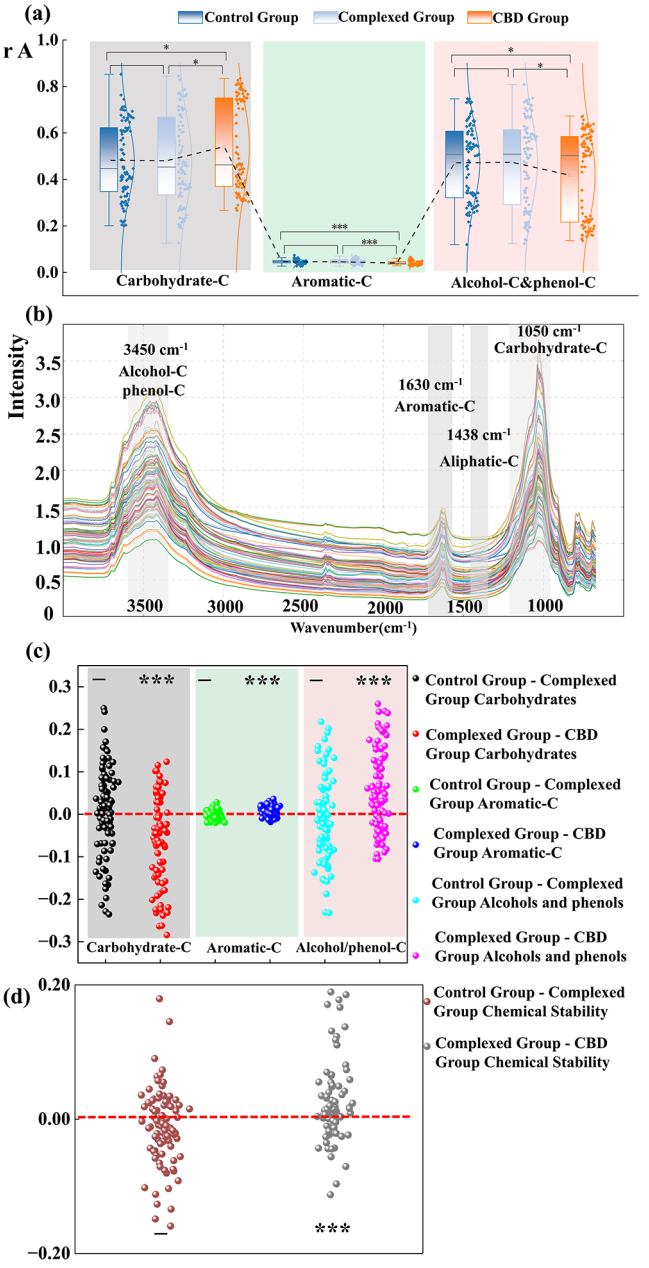


Figure 6. Fourier transform infrared (FTIR) spectra. (a) Boxplots showing the mean relative peak area proportions of four functional groups, normalized to the total peak area. The boxplots display the mean (solid square), median (center line), 25th and 75th percentiles (box boundaries), and 1.5 × interquartile range (whiskers), with individual data points overlaid as solid dots. Significance markers from *t*-tests were added to compare different treatment groups for the three functional groups, where * indicates $p < 0.05$, ** indicates $p < 0.01$, and *** indicates $p < 0.001$, no asterisk indicates no significant difference. (b) FTIR absorption spectra. (c) Differences in the relative peak areas of three functional groups among experimental treatments. The *y*-axis represents changes in the relative peak area of each functional group before and after treatment in each group. A one-sample *t*-test was used to compare the values against zero, where—indicates no significant difference, * indicates $p < 0.05$, ** indicates $p < 0.01$, and *** indicates $p < 0.001$. (d) Variations in chemical stability among experimental treatments. The *y*-axis represents changes in chemical stability before and after treatment in each group. A one-sample *t*-test was used to compare the values against zero, where—indicates no significant difference, * indicates $p < 0.05$, ** indicates $p < 0.01$, and *** indicates $p < 0.001$.

Downloaded from pubs.acs.org/esthag/article-pdf/60/37/26504/6844071/4/acs.est.6c07771.pdf by NANJING UNIV user on 25 September 2026

https://doi.org/10.1021/acs.est.6c07771
Environ. Sci. Technol. 2026, 60, 26504−26514

field-based evidence for the redistribution of OC between different Fe_R-bound fractions but also highlight the distinct roles of Fe_R phases in the long-term burial and preservation of the OC.

■ ASSOCIATED CONTENT

Data Availability Statement

The data supporting this article are openly available at Zenodo, 10.5281/zenodo.22240240

Supporting Information

The Supporting Information is available free of charge at https://pubs.acs.org/doi/10.1021/acs.est.6c07771.

Analysis data for Fe-OC fractions (XLSX)

Experimental determination methods for OC, carbon isotopes, and porewater (Text S1), a discussion on the extraction of complexed iron-bound OC (Fe_p-OC; Text S2), a detailed account of the experimental procedures employed in this study (Text S3, Figure S1), data figures for OC and carbon isotopes (Figures S2 and S3), the proportions of various iron fractions in Fe_R, and the percentage of Fe-bound OC in Fe_R-OC (Figure S4), the detailed methods and results of the analysis of the laboratory anaerobic incubation experiment (Text S4), a map of sediment sampling locations for the laboratory incubation experiment (Figure S5), and the results of the laboratory incubation experiment (Figure S6) (PDF)

■ AUTHOR INFORMATION

Corresponding Authors

Chenglong Wang − *School of Geography and Ocean Science, Ministry of Education Key Laboratory for Coast and Island Development, Nanjing University, Nanjing 210023, China*; Email: clwang@nju.edu.cn

Xinqing Zou − *School of Geography and Ocean Science, Ministry of Education Key Laboratory for Coast and Island Development, Nanjing University, Nanjing 210023, China; Collaborative Innovation Center of South China Sea Studies, Nanjing University, Nanjing 210023, China; School of Geography and Environmental Sciences, Hainan Normal University, Haikou 571158, China*; orcid.org/0000-0003-3314-9701; Email: zouxq@nju.edu.cn

Authors

Zicheng Chen − *School of Geography and Ocean Science, Ministry of Education Key Laboratory for Coast and Island Development, Nanjing University, Nanjing 210023, China*

Zhuoyue Zhang − *School of Geography and Ocean Science, Ministry of Education Key Laboratory for Coast and Island Development, Nanjing University, Nanjing 210023, China*

Qiujun An − *School of Geography and Ocean Science, Ministry of Education Key Laboratory for Coast and Island Development, Nanjing University, Nanjing 210023, China*

Tianyu Chen − *State Key Laboratory of Critical Earth Material Cycling and Mineral Deposits, School of Earth Sciences and Engineering, Nanjing University, Nanjing 210023, China*; orcid.org/0000-0002-3061-7170

Chendong Ge − *School of Geography and Ocean Science, Ministry of Education Key Laboratory for Coast and Island Development, Nanjing University, Nanjing 210023, China; Collaborative Innovation Center of South China Sea Studies, Nanjing University, Nanjing 210023, China*

Manqing Zhang − *School of Geography and Ocean Science, Ministry of Education Key Laboratory for Coast and Island Development, Nanjing University, Nanjing 210023, China*

Yaping Wang − *School of Geography and Ocean Science, Ministry of Education Key Laboratory for Coast and Island Development, Nanjing University, Nanjing 210023, China*; orcid.org/0000-0002-8771-465X

Complete contact information is available at: https://pubs.acs.org/10.1021/acs.est.6c07771

Author Contributions

The manuscript was written through contributions of all authors. All authors have given approval to the final version of the manuscript. Conceptualization: Zicheng Chen, Chenglong Wang, and Xinqing Zou. Formal analysis: Zhuoyue Zhang, Qiujun An, Manqing Zhang, Chendong Ge, and Yaping Wang. Funding acquisition: Zicheng Chen, Chenglong Wang and Xinqing Zou. Investigation: Zicheng Chen and Qiujun An. Writing—review & editing: Zicheng Chen, Chenglong Wang, Zhuoyue Zhang, Qiujun An, Tianyu Chen, Yaping Wang, and Xinqing Zou.

Funding

This work was supported by the National Natural Science Foundation of China (Grant Nos. 42576210 and 42106056), the Innovation Project of Natural Resources Science and Technology of Jiangsu Province (JSZRKJ202423), and the Fundamental Research Funds for the Central Universities (Grant Nos. 0209−14380134 and 14370414), and the Postgraduate Research & Practice Innovation Program of Jiangsu Province (Grant 26CXJH0242).

Notes

The authors declare no competing financial interest.

■ ACKNOWLEDGMENTS

The authors gratefully acknowledge the financial support provided by the National Natural Science Foundation of China (Grant Nos. 42576210 and 42106056), the Innovation Project of Natural Resources Science and Technology of Jiangsu Province (JSZRKJ202423), and the Fundamental Research Funds for the Central Universities (Grant Nos. 0209−14380134 and 14370414), and the Postgraduate Research & Practice Innovation Program of Jiangsu Province (Grant 26CXJH0242). We also sincerely thank the NSFC Shiptime Sharing Project for funding the open research cruise NORC2025-01. We are grateful to the crew and researchers aboard the RV "Lanhai 101" for their valuable assistance with field sampling and on-site data collection of Core H09, H25, H27, H28, and H29 during the cruise.

■ REFERENCES

(1) Burdige, D. J. Preservation of Organic Matter in Marine Sediments: Controls, Mechanisms, and an Imbalance in Sediment Organic Carbon Budgets? *Chem. Rev.* **2007**, *107* (2), 467−485.

(2) Emerson, S.; Hedges, J. I. Processes Controlling the Organic Carbon Content of Open Ocean Sediments. *Paleoceanography* **1988**, *3* (5), 621−634.

(3) LaRowe, D. E.; Arndt, S.; Bradley, J. A.; Estes, E. R.; Hoarfrost, A.; Lang, S. Q.; Lloyd, K. G.; Mahmoudi, N.; Orsi, W. D.; Shah Walter, S. R.; Steen, A. D.; Zhao, R. The Fate of Organic Carbon in

Downloaded from pubs.acs.org/esthag/article-pdf/60/37/26504/6844071/4/acs.est.6c07771.pdf by NANJING UNIV user on 25 September 2026

Marine Sediments - New Insights from Recent Data and Analysis. *Earth Sci. Rev.* **2020**, *204*, 103146.
(4) Homoky, W. B.; Conway, T. M.; John, S. G.; König, D.; Deng, F.; Tagliabue, A.; Mills, R. A. Iron Colloids Dominate Sedimentary Supply to the Ocean Interior. *Proc. Natl. Acad. Sci. U.S.A.* **2021**, *118* (13), No. e2016078118.
(5) Johnson, K.; Purvis, G.; Lopez-Capel, E.; Ojeda, J.; et al. Towards a Mechanistic Understanding of Carbon Stabilization in Manganese Oxides. *Nat. Commun* **2015**, *6*, 7628.
(6) Canfield, D. E.; Thamdrup, B.; Hansen, J. W. The Anaerobic Degradation of Organic Matter in Danish Coastal Sediments: Iron Reduction, Manganese Reduction, and Sulfate Reduction. *Geochim. Cosmochim. Acta* **1993**, *57* (16), 3867−3883.
(7) Lovley, D. R.; Holmes, D. E.; Nevin, K. P. Dissimilatory Fe(III) and Mn(IV). *Reduction* **2004**, *49*, 219−286.
(8) Lalonde, K.; Mucci, A.; Ouellet, A.; Gélinas, Y. Preservation of Organic Matter in Sediments Promoted by Iron. *Nature* **2012**, *483* (7388), 198−200.
(9) Riedel, T.; Zak, D.; Biester, H.; Dittmar, T. Iron Traps Terrestrially Derived Dissolved Organic Matter at Redox Interfaces. *Proc. Natl. Acad. Sci. U.S.A.* **2013**, *110* (25), 10101−10105.
(10) Shields, M. R.; Bianchi, T. S.; Gélinas, Y.; Allison, M. A.; Twilley, R. R. Enhanced Terrestrial Carbon Preservation Promoted by Reactive Iron in Deltaic Sediments. *Geophys. Res. Lett.* **2016**, *43* (3), 1149−1157.
(11) Chen, Y.; Dong, L.; Sui, W.; Niu, M.; Cui, X.; Hinrichs, K.-U.; Wang, F. Cycling and Persistence of Iron-Bound Organic Carbon in Subseafloor Sediments. *Nat. Commun.* **2024**, *15* (1), 6370.
(12) Hu, Y.; Li, K.; Faust, J. C.; Peckmann, J.; Zhang, D.; Chen, L.; Liang, Q.; Chen, D.; Feng, D. Stability of Reactive Iron-bound Organic Carbon during Sulfidization of Iron Oxides: Insights from Methane-seep Sediments. *Geophys. Res. Lett.* **2025**, *52* (8), No. e2024GL112119.
(13) Voggenreiter, E.; Thomasarrigo, L.; Kilian, J.; Straub, D.; Friedel, M.; Stahl, M.; Kappler, A.; Joshi, P. Reduction of Iron-Organic Carbon Associations Shifts Net Greenhouse Gas Release after Initial Permafrost Thaw. *Soil Biol. Biochem.* **2025**, *203*, 109735.
(14) Chen, C.; Hall, S. J.; Coward, E.; Thompson, A. Iron-Mediated Organic Matter Decomposition in Humid Soils Can Counteract Protection. *Nat. Commun.* **2020**, *11* (1), 2255.
(15) Patzner, M. S.; Mueller, C. W.; Malusova, M.; Baur, M.; Nikeleit, V.; Scholten, T.; Hoeschen, C.; Byrne, J. M.; Borch, T.; Kappler, A.; Bryce, C. Iron Mineral Dissolution Releases Iron and Associated Organic Carbon during Permafrost Thaw. *Nat. Commun.* **2020**, *11* (1), 6329.
(16) Liang, L.; Wang, Y.; Sivan, O.; Wang, F. Metal-Dependent Anaerobic Methane Oxidation in Marine Sediment: Insights from Marine Settings and Other Systems. *Sci. China Life Sci.* **2019**, *62* (10), 1287−1295.
(17) Liang, L.; Vigderovich, H.; Sivan, O.; Hou, J.; Niu, M.; Yorshansky, O.; Zhang, T.; Bosco-Santos, A.; Wang, F. Iron (Oxyhydr)Oxides Shift the Methanogenic Community in Deep Sea Methanic Sediment - Insights from Long-Term High-Pressure Incubations. *Sci. Total Environ.* **2022**, *848*, 157590.
(18) Melton, E. D.; Swanner, E. D.; Behrens, S.; Schmidt, C.; Kappler, A. The Interplay of Microbially Mediated and Abiotic Reactions in the Biogeochemical Fe Cycle. *Nat. Rev. Microbiol.* **2014**, *12* (12), 797−808.
(19) Ghaisas, N. A.; Maiti, K.; Roy, A. Iron-Mediated Organic Matter Preservation in the Mississippi River-Influenced Shelf Sediments. *JGR Biogeosciences* **2021**, *126* (4), No. e2020JG006089.
(20) Sun, C.-H.; Zhu, M.-X.; Ma, W.-W.; Sun, Z.-L.; Zhang, X.-R.; Ding, K.-Y.; Liu, S.-H. Examining Bulk and Iron-Associated Organic Carbon through Depth in Margin Sea Sediments (China) under Contrasting Depositional Settings: Chemical and NEXAFS Spectral Characterization. *J. Mar. Syst.* **2020**, *207*, 103344.
(21) Dicen, G. P.; Navarrete, I. A.; Rallos, R. V.; Salmo, S. G.; Garcia, M. C. A. The Role of Reactive Iron in Long-Term Carbon Sequestration in Mangrove Sediments. *J. Soils Sediments* **2019**, *19* (1), 501−510.
(22) Raiswell, R.; Canfield, D. E. Sources of Iron for Pyrite Formation in Marine Sediments. *Am. J. Sci.* **1998**, *298* (3), 219−245.
(23) Schwertmann, U. Solubility and Dissolution of Iron Oxides. *Plant Soil* **1991**, *130* (1−2), 1−25.
(24) Ruiz, F.; Bernardino, A. F.; Queiroz, H. M.; Otero, X. L.; Rumpel, C.; Ferreira, T. O. Iron's Role in Soil Organic Carbon (de)Stabilization in Mangroves under Land Use Change. *Nat. Commun.* **2024**, *15* (1), 10433.
(25) de Koff, J. P.; Anderson, M. A.; Amrhein, C. Geochemistry of Iron in the Salton Sea, California. *Hydrobiologia* **2008**, *604* (1), 111−121.
(26) Zhihao, W.; Bingnian, Z.; Hanzhong, J.; Ziyan, L. Iron-Bound Organic-Carbon Dynamics in a Fertilized Agriustoll. *Soil Tillage Res.* **2026**, *258*, 107027.
(27) Xue, B.; Huang, L.; Huang, Y.; Ali Kubar, K.; Li, X.; Lu, J. Straw Management Influences the Stabilization of Organic Carbon by Fe (Oxyhydr)Oxides in Soil Aggregates. *Geoderma* **2020**, *358*, 113987.
(28) Wu, Y.; Zhang, J.; Liu, S. M.; Zhang, Z. F.; Yao, Q. Z.; Hong, G. H.; Cooper, L. Sources and Distribution of Carbon within the Yangtze River System. *Estuarine Coastal Shelf Sci.* **2007**, *71* (1−2), 13−25.
(29) Yang, Z.; Wang, H.; Saito, Y.; Milliman, J. D.; Xu, K.; Qiao, S.; Shi, G. Dam Impacts on the Changjiang (Yangtze) River Sediment Discharge to the Sea: The Past 55 Years and after the Three Gorges Dam. *Water Resour. Res.* **2006**, *42* (4), 2005WR003970.
(30) Zhu, Q.; Xing, F.; Wang, Y. P.; Syvitski, J.; Overeem, I.; Guo, J.; Li, Y.; Tang, J.; Yu, Q.; Gao, J.; Gao, S. Hidden Delta Degradation Due to Fluvial Sediment Decline and Intensified Marine Storms. *Sci. Adv.* **2024**, *10* (18), No. eadk1698.
(31) Yuan, D.; Zhu, J.; Li, C.; Hu, D. Cross-Shelf Circulation in the Yellow and East China Seas Indicated by MODIS Satellite Observations. *J. Mar. Syst.* **2008**, *70* (1−2), 134−149.
(32) Ai, L.; Han, Z.; Wu, X.; Liu, S.; Bi, N.; Saito, Y.; Shi, X.; Wang, H. How Did the Climate and Human Activities Modulate the Sedimentary Evolution of the Central Yellow Sea Mud, China. *Asian J. Earth Sci.* **2022**, *235*, 105299.
(33) Zhang, Z.; Lu, M.; Wang, C.; Zhang, C.; Lin, B.; Liao, Q.; Qiu, P.; Zou, X. Divergent Responses of Organic Carbon to Sedimentary Environment Transformation in a River-dominated Marginal Sea. *JGR Biogeosciences* **2024**, *129* (11), No. e2024JG008034.
(34) Zhang, Y.; Wang, H.; Hu, L.; Xing, L.; Li, G.; Wu, X. Different Pacemakers of Marine Organic Carbon Burial in the North Yellow Sea from the Early to Late Holocene. *Palaeogeogr., Palaeoclimatol., Palaeoecol.* **2024**, *652*, 112408.
(35) Hamm, R. E.; Shull, C. M.; Grant, D. M. Citrate Complexes with Iron(II) and Iron(III)[1]. *J. Am. Chem. Soc.* **1954**, *76* (8), 2111−2114.
(36) Karlsson, T.; Persson, P. Complexes with Aquatic Organic Matter Suppress Hydrolysis and Precipitation of Fe(III). *Chem. Geol.* **2012**, *322*−*323*, 19−27.
(37) Chen, C.; Dynes, J. J.; Wang, J.; Sparks, D. L. Properties of Fe-Organic Matter Associations via Coprecipitation versus Adsorption. *Environ. Sci. Technol.* **2014**, *48* (23), 13751−13759.
(38) McKeague, J. A. AN EVALUATION OF 0.1 *M* PYROPHOSPHATE AND PYROPHOSPHATE-DITHIONITE IN COMPARISON WITH OXALATE AS EXTRACTANTS OF THE ACCUMULATION PRODUCTS IN PODZOLS AND SOME OTHER SOILS. *Can. J. Soil Sci.* **1967**, *47* (2), 95−99.
(39) Calderón, F.; Haddix, M.; Conant, R.; Magrini-Bair, K.; Paul, E. Diffuse-Reflectance Fourier-Transform Mid-Infrared Spectroscopy as a Method of Characterizing Changes in Soil Organic Matter. *Soil Sci. Soc. Am. J.* **2013**, *77* (5), 1591−1600.
(40) Liao, Q.; Yuan, F.; Fan, Q.; Chen, H.; Wang, Y.; Zhang, C.; Lu, C.; Qiu, P.; Wang, C.; Zou, X. Plant- and Microbial-Mediated Soil Organic Carbon Accumulation in Spartina Alterniflora Salt Marshes. *Catena* **2024**, *237*, 107777.

Downloaded from pubs.acs.org/esthag/article-pdf/60/37/26504/6844071 4/acs.est.6c07771.pdf by NANJING UNIV user on 25 September 2026

(41) Shao, P.; Liang, C.; Lynch, L.; Xie, H.; Bao, X. Reforestation Accelerates Soil Organic Carbon Accumulation: Evidence from Microbial Biomarkers. *Soil Biol. Biochem.* **2019**, *131*, 182−190.
(42) Hou, Y.; Chen, Y.; Chen, X.; He, K.; Zhu, B. Changes in Soil Organic Matter Stability with Depth in Two Alpine Ecosystems on the Tibetan Plateau. *Geoderma* **2019**, *351*, 153−162.
(43) Wagai, R.; Mayer, L. M. Sorptive Stabilization of Organic Matter in Soils by Hydrous Iron Oxides. *Geochim. Cosmochim. Acta* **2007**, *71* (1), 25−35.
(44) Duan, X.; Li, Z.; Wang, S.; Mason-Jones, K.; Wei, L.; Chen, X.; Wu, J.; Ge, T.; Zhu, Z. Stability of Iron-Carbon Complexes Determines Carbon Sequestration Efficiency in Iron-Rich Soils. *Soil Biol. Biochem.* **2025**, *203*, 109718.
(45) Zhao, B.; Yao, P.; Bianchi, T. S.; Wang, X.; Yu, Z. Contrasting Controls of Particulate Organic Carbon Composition and Age from Riverine to Coastal Sediments of Eastern China Marginal Seas. *Chem. Geol.* **2023**, *624*, 121429.
(46) He, B.; Dai, M.; Huang, W.; Liu, Q.; Chen, H.; Xu, L. Sources and Accumulation of Organic Carbon in the Pearl River Estuary Surface Sediment as Indicated by Elemental, Stable Carbon Isotopic, and Carbohydrate Compositions. *Biogeosciences* **2010**, *7* (10), 3343−3362.
(47) Raiswell, R.; Anderson, T. F. Reactive Iron Enrichment in Sediments Deposited beneath Euxinic Bottom Waters: Constraints on Supply by Shelf Recycling; *Mineral Deposits and Earth Evolution*; McDonald, I., Boyce, A. J., Butler, I. B., Herrington, R. J., Polya, D. A., Eds.; Geological Soc Publishing House: Bath, 2005; Vol. *248*, pp 179−194.10.1144/GSL.SP.2005.248.01.10.
(48) Retschko, A.-K.; Vosteen, P.; Plass, A.; Welter, E.; Scholz, F. Comparison of Sedimentary Iron Speciation Obtained by Sequential Extraction and X-Ray Absorption Spectroscopy. *Mar. Chem.* **2023**, *252*, 104249.
(49) Faust, J. C.; Tessin, A.; Fisher, B. J.; Zindorf, M.; Papadaki, S.; Hendry, K. R.; Doyle, K. A.; März, C. Millennial Scale Persistence of Organic Carbon Bound to Iron in Arctic Marine Sediments. *Nat. Commun.* **2021**, *12* (1), 275.
(50) Rickard, D.; Luther, G. W. Chemistry of Iron Sulfides. *Chem. Rev.* **2007**, *107* (2), 514−562.
(51) Bowles, J. F. W. R. M. Cornell and U. Schwertmann The Iron Oxides: Structure, Properties Reactions Occurrence and Uses. Weinheim and New York (VCH Verlagsgeseiischaft mbH) 1996, Xxxi + 573 Pp. Price DM 328.00. ISBN 3-527-28576-8. *Mineral. Mag.* **1997**, *61* (408), 740−741.
(52) Jelavić, S.; Mitchell, A. C.; Sand, K. K. Fate of Organic Compounds during Transformation of Ferrihydrite in Iron Formations. *Geochem. Persp. Lett.* **2020**, *15*, 25−29.
(53) Zhu, M.-X.; Shi, X.; Yang, G.-P.; li, T.; Lü, R. Relative Contributions of Various Early Diagenetic Pathways to Mineralization of Organic Matter in Marine Sediments: An Overview. *Adv. Earth Sci* **2011**, *26* (4), 355.
(54) Faust, J. C.; Ascough, P.; Hilton, R. G.; Stevenson, M. A.; Hendry, K. R.; März, C. New Evidence for Preservation of Contemporary Marine Organic Carbon by Iron in Arctic Shelf Sediments. *Environ. Res. Lett.* **2023**, *18* (1), 014006.
(55) Song, G.; Liu, S.; Zhu, Z.; Zhai, W.; Zhu, C.; Zhang, J. Sediment Oxygen Consumption and Benthic Organic Carbon Mineralization on the Continental Shelves of the East China Sea and the Yellow Sea. *Deep Sea Res., Part II* **2016**, *124*, 53−63.
(56) O'Loughlin, E. J.; Gorski, C. A.; Scherer, M. M.; Boyanov, M. I.; Kemner, K. M. Effects of Oxyanions, Natural Organic Matter, and Bacterial Cell Numbers on the Bioreduction of Lepidocrocite (γ-FeOOH) and the Formation of Secondary Mineralization Products. *Environ. Sci. Technol.* **2010**, *44* (12), 4570−4576.
(57) Shao, Y.; Sun, S.; Ding, S.; Peng, Y.; Gu, X.; Mochida, K.; He, S. Fate of Organic Carbon Shaped by Iron Minerals in Coastal Wetlands: Mechanisms and Implications. *Environ. Sci. Technol.* **2026**, *60* (14), 10377−10392.
(58) Li, Z.; Li, X.; Jiao, B.; Yang, Y.; Wang, H.; Gu, L.; Ai, H.; Cheng, H.; Cheng, S. Redox Oscillations in Riparian Zone Stimulate Carbon Loss by Enhancing Microbial Respiration. *Water Res.* **2026**, *296*, 125672.
(59) Canfield, D. E. Reactive Iron in Marine Sediments. *Geochim. Cosmochim. Acta* **1989**, *53* (3), 619−632.
(60) Philippe, A.; Schaumann, G. E. Interactions of Dissolved Organic Matter with Natural and Engineered Inorganic Colloids: A Review. *Environ. Sci. Technol.* **2014**, *48* (16), 8946−8962.
(61) Bao, Y.; Bolan, N. S.; Lai, J.; Wang, Y.; Jin, X.; Kirkham, M. B.; Wu, X.; Fang, Z.; Zhang, Y.; Wang, H. Interactions between Organic Matter and Fe (Hydr)Oxides and Their Influences on Immobilization and Remobilization of Metal(Loid)s: A Review. *Crit. Rev. Environ. Sci. Technol.* **2022**, *52* (22), 4016−4037.
(62) Gordon, E. S.; Goñi, M. A. Sources and Distribution of Terrigenous Organic Matter Delivered by the Atchafalaya River to Sediments in the Northern Gulf of Mexico. *Geochim. Cosmochim. Acta* **2003**, *67* (13), 2359−2375.
(63) Kaiser, K.; Guggenberger, G. The Role of DOM Sorption to Mineral Surfaces in the Preservation of Organic Matter in Soils. *Org. Geochem.* **2000**, *31* (7), 711−725.
(64) Arnarson, T. S.; Keil, R. G. Changes in Organic Matter−Mineral Interactions for Marine Sediments with Varying Oxygen Exposure Times. *Geochim. Cosmochim. Acta* **2007**, *71* (14), 3545−3556.
(65) Li, Q.; Li, L.; Du, H.; Lin, X.; Hu, W.; Li, Y. Soil Conditioners Promote the Formation of Fe-Bound Organic Carbon and Its Stability. *J. Environ. Manage.* **2024**, *349*, 119480.
(66) Han, L.; Sun, K.; Keiluweit, M.; Yang, Y.; Yang, Y.; Jin, J.; Sun, H.; Wu, F.; Xing, B. Mobilization of Ferrihydrite-Associated Organic Carbon during Fe Reduction: Adsorption versus Coprecipitation. *Chem. Geol.* **2019**, *503*, 61−68.
(67) Huang, X.; Tang, H.; Kang, W.; Yu, G.; Ran, W.; Hong, J.; Shen, Q. Redox Interface-Associated Organo-Mineral Interactions: A Mechanism for C Sequestration under a Rice-Wheat Cropping System. *Soil Biol. Biochem.* **2018**, *120*, 12−23.
(68) Hu, L.; Ji, Y.; Zhao, B.; Liu, X.; Du, J.; Liang, Y.; Yao, P. The Effect of Iron on the Preservation of Organic Carbon in Marine Sediments and Its Implications for Carbon Sequestration. *Sci. China Earth Sci.* **2023**, *66* (9), 1946−1959.
(69) Zhao, B.; Yao, P.; Bianchi, T. S.; Shields, M. R.; Cui, X. Q.; Zhang, X. W.; Huang, X. Y.; Schröder, C.; Zhao, J.; Yu, Z. G. The Role of Reactive Iron in the Preservation of Terrestrial Organic Carbon in Estuarine Sediments. *JGR Biogeosciences* **2018**, *123* (12), 3556−3569.

Downloaded from pubs.acs.org/esthag/article-pdf/60/37/26504/6844071 4/acs.est.6c07771.pdf by NANJING UNIV user on 25 September 2026

https://doi.org/10.1021/acs.est.6c07771
Environ. Sci. Technol. 2026, 60, 26504−26514